Impact regimes of nanodroplets impacting nanopillared surfaces

Shu-Hang Lv,[1,2,5] Fang-Fang Xie,[1,2] Yan-Ru Yang,[1,2] Duu-Jong Lee,[3,4] Xiao-Dong Wang,[1,2,*] and Yuan-Yuan Duan[5,†]

[1]*State Key Laboratory of Alternate Electrical Power System with Renewable Energy Sources, North China Electric Power University, Beijing 102206, China*

[2]*Research Center of Engineering Thermophysics, North China Electric Power University, Beijing 102206, China*

[3]*Department of Chemical Engineering, National Taiwan University, Taipei 106, Taiwan*

[4]*Department of Mechanical Engineering, City University of Hong Kong, Kowloon Tang, Hong Kong*

[5]*Key Laboratory for Thermal Science and Power Engineering of Ministry of Education, Beijing Key Laboratory for CO_2 Utilization and Reduction Technology, Tsinghua University, Beijing 100084, China*

(Received 13 August 2021; accepted 8 March 2022; published 28 March 2022)

In this study, a phase diagram is constructed for the impact of nanodroplets on nanopillared surfaces via molecular dynamics simulations. Four impact regimes, i.e., first nonbouncing (1NB), bouncing, second nonbouncing (2NB), and sticky, are discovered at various pillar heights and Weber numbers. The impact regimes are compared with those at the macroscale, and several significant differences are distinguished. The differences are attributed to the significantly enhanced viscous effect, the modified viscous dissipation mechanism, and the altered wetting transition mechanism. The impact regimes are found to strongly depend on the properties of surfaces. On monostable Wenzel surfaces (small pillar heights), the sticky regime is the only regime; on metastable coexisting Cassie–Wenzel surfaces (moderate pillar heights), the 1NB and sticky regimes successively take place with increasing Weber numbers; and on monostable Cassie surfaces (large pillar heights), the sticky regime disappears, but two new regimes, i.e., the bouncing and 2NB regimes, appear. The boundaries between the 1NB and sticky regimes, between the 1NB and 2NB regimes, and between the bouncing and 2NB regimes are all related to the formation of a partial wetting state, in which the central gaps beneath the nanodroplet are intruded and completely wetted. The wetting transition at the nanoscale does not follow the macroscale depinning mechanism. Therefore, a theoretical model is developed to understand the wetting transition mechanism at the nanoscale and thus predicting the critical Weber number for triggering the wetting transition, yielding $We_{cr}^{1/2} \sim -h^* \cos\theta_i$, which well describes the boundaries mentioned above.

DOI: 10.1103/PhysRevFluids.7.034203

I. INTRODUCTION

The impact of droplets on solid surfaces is a ubiquitous physical phenomenon in nature and industrial applications. When impacting solid surfaces, droplets will deform and wet the surfaces. The impact dynamics of droplets have attracted extensive interest due to their wide applications, such as anti-icing [1,2], self-cleaning [3–5], inkjet printing [6,7], spray cooling [8,9], and so forth.

*wangxd99@gmail.com
†yyduan@tsinghua.edu.cn

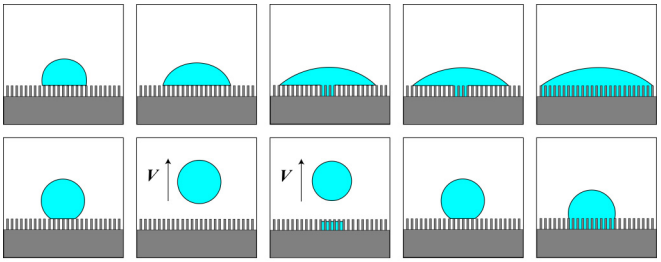

FIG. 1. Impact regimes for macroscale droplets impacting textured surfaces.

In recent years, there is growing interest in the study of impact regimes of droplets on textured surfaces, especially on pillared surfaces, owing to their important role in applications of superhydrophobic surfaces [10–13]. Impact regimes of droplets and dynamic behaviors in different regimes on textured surfaces have been studied experimentally [14–24], theoretically [25–28], and numerically [29–32]. Wetting states of droplets are particularly focused on in previous studies due to their huge influence on the impact behaviors and resulting impact regimes. Wetting states on rough surfaces can be divided into two different types, i.e., the Cassie state [33] and Wenzel state [34]. When droplets stay in the Cassie state, the trapped air pockets in the surface asperities decrease the area of the liquid-solid interface, leading to low adhesive works and high apparent contact angles. On the contrary, droplets in the Wenzel state that fully wet the surface asperities show lower apparent contact angles, larger contact angle hysteresis, and preferences to adhere. Impacting droplets in the Cassie state can bounce off from superhydrophobic surfaces [10–13]. However, previous studies have demonstrated that the Cassie state is often metastable [14,15,35], and hence, external stimuli such as impact [14–23], evaporation [36], electric field [37], and vibration [38] can cause the wetting transition from the Cassie state to the Wenzel state, resulting in high adhesion and thus suppressing rebounding.

According to the wetting states and impact outcomes, five impact regimes have been identified for macroscale droplets on pillared surfaces, including first nonbouncing (1NB), bouncing, partial penetrated bouncing (PPB), second nonbouncing (2NB), and sticky, as shown in Fig. 1. Bartolo *et al.* [14] studied the impact of droplets on micropillared superhydrophobic surfaces and found that droplets could bounce off surfaces only at intermediate velocities. They therefore discovered three impact regimes at various impact velocities, i.e., 1NB, bouncing, and sticky. In the 1NB regime, the droplets with low-impact velocities did not transition to the Wenzel state and eventually stayed on surfaces in the Cassie state. As the impact velocity increased, droplets would overcome the adhesive work to bounce off surfaces. However, when the impact velocity further increased and exceeded a limit, a sharp decrease in the instantaneous contact angle hindered the rebounding, leading to the occurrence of the sticky regime. Despite no direct experimental evidence, this result implied that a sufficiently high impact velocity would cause the wetting transition from the Cassie state to the Wenzel state, thereby preventing the droplet rebounding. To predict the critical velocity of wetting transition, Bartolo *et al.* [14] considered the dynamic pressure, $P_D \sim \rho V^2/2$, as the decisive factor of wetting transition, where ρ is the liquid density and V is the impact velocity. When the dynamic pressure of droplets exceeds the impalement pressure, P_{imp}, the substrate bottom will be wetted, leading to the wetting transition from the Cassie state to the Wenzel state. In the subsequent studies [17,21,22,29,30], two new impact regimes are identified, i.e., 2NB and PPB. The water hammer pressure, P_{WH}, is believed to play an important role in the two impact regimes [20,21]. When impacting droplets come into contact with solid surfaces, the water hammer pressure, which is often larger than the dynamic pressure, would be generated in the initial stage of spreading due to the liquid compression. Hence, when a droplet impacts a pillared surface, the pressure near the

center of the droplet is larger due to the water hammer pressure, whereas the pressure decreases gradually away from the center. In case that the water hammer pressure exceeds the impalement pressure while the dynamic pressure does not, only the liquid in the center of the droplet can intrude into asperities, leading to a partial wetting state, which is an intermediate state between the Cassie and Wenzel states. In such circumstances, two outcomes are observed. One outcome is that the intruding liquid cannot leave the intruded asperities; the droplet merely bounces off the surface partially, referred to as the PPB. The other outcome is that the intruding liquid extrudes from the asperities, but the droplet stays on the surface instead of bouncing, referred to as the 2NB.

According to the difference in wetting states, textured surfaces can be divided into three categories. On some textured surfaces, referred to as Wenzel surfaces, the Wenzel state has the globally energetic minimum so that the equilibrated droplet is always in the Wenzel state regardless of its initial wetting state. On the contrary, on Cassie surfaces, the Cassie state is globally energetic minimum, and hence, the equilibrated droplet is always in the Cassie state. The third category of textured surfaces is called metastable Cassie surfaces or coexisting Cassie–Wenzel surfaces, on which the equilibrated droplet can be either in the Cassie state or in the Wenzel state, depending on the initial wetting state or external stimuli. It is worth noting that the above-mentioned five impact regimes were observed merely on coexisting Cassie–Wenzel surfaces. However, on Cassie surfaces or Wenzel surfaces, droplets can spontaneously transition to the globally stable state regardless of their initial state and external stimuli. As a consequence, impact regimes may be different from those on coexisting Cassie–Wenzel surfaces. This speculation has been verified by a recent study [39], in which the impact of droplets was experimentally studied on a monostable Cassie surface. Although the Cassie-to-Wenzel wetting transition had taken place, there were no liquid residues in asperities after droplets bounced off the surface. This bouncing regime differs from both the bouncing and PPB regimes. Therefore, more efforts should be devoted to revealing bouncing regimes and corresponding impact dynamics on monostable Cassie and Wenzel surfaces.

Because of its scientific and engineering importance, the wetting transition has been extensively studied in recent decades. Two kinds of mechanisms were proposed by Bartolo *et al.* [14], who studied the wetting transition on pillared surfaces. They presented that the impalement pressure could be used as a criterion to determine whether the wetting transition would take place, and hence, they measured the impalement pressures for various pillar heights. Based on the fact that the impalement pressure increased with the pillar height at small heights while remained constant at large ones, they believed that the impalement pressure was determined by different mechanisms, i.e., a sag mechanism for small pillar heights and a depinning mechanism for higher pillar heights. The two mechanisms have been widely accepted to interpret the wetting transition on textured surfaces [17,20,23,27,36,37]. In the sag mechanism, the curved liquid-air interfaces between pillars directly touch the bottom of the substrate, whereas the contact lines are pinned at the tops of pillars until the bottom of the substrate is wetted. Thus, the impalement pressure is determined by the pressure that makes the liquid-air interfaces touch the bottom of the substrate, thereby increasing with the pillar height. However, in the depinning mechanism, the pillar height is so large that the liquid-air interfaces cannot directly wet the bottom of the substrate without depinning of the contact lines. The critical pressure for depinning depends on the intrinsic contact angle of surfaces, spacing between two adjacent pillars, and liquid surface tension so that the impalement pressure is independent of the pillar height. It should be noted that parts of regime boundaries for impacting droplets on textured surfaces are identified by the wetting transition, and hence, the two mechanisms provide useful information to understand the transition between impact regimes.

With the rapid development of nanotechnologies, the impact of nanodroplets has received increasing attention owing to its wide applications in nanoprinting [40], nanospray [41], and nanocoating [42]. Up to now, experiments of nanodroplet impact still face huge challenges, and hence, molecular dynamics (MD) simulations have become a popular and powerful tool. MD simulations have been implemented to investigate various nanoscale phenomena, such as evaporation of nanodroplets [43], coalescence-induced nanodroplet jumping [44], and thermal fluctuations in nanoscale thin liquid films [45,46]. Recently, the impact dynamics of nanodroplets on

smooth surfaces were investigated via MD simulations from many aspects, including the maximum spreading radius [47–52], spreading time [53], bouncing condition [32], contact time [54,55], and so forth. These studies indicated that the impact dynamics of nanodroplets greatly differ from those of macroscale droplets owing to scale effects. Two scale effects have been clarified. One is the increased viscous effect with decreasing droplet sizes, which can be characterized by the Ohnesorge number, $Oh = \mu/(\rho D_0 \gamma)^{1/2}$, describing the ratio of viscous to inertial-capillary forces. For example, the Ohnesorge number increases from 0.003 32 to 1.05 when the diameter of a water droplet decreases from 1 mm to 10 nm, showing a significantly enhanced viscous effect. The other is the altered mechanism of viscous dissipation from macroscale to nanoscale droplets. The dissipation occurs only in the boundary layer for the impact of millimeter-sized droplets but within the whole droplet for the impact of nanodroplets [47–52]. For the impact of nanodroplets on nanostructured surfaces, a new scale effect may be generated. The feature size of nanostructures is comparable to that of nanodroplets. As a result, once the Cassie-to-Wenzel wetting transition takes place for impacting nanodroplets, the decrease in the volume of droplets above nanostructures cannot be neglected, which may modify the spreading and retraction dynamics of droplets. On the other hand, impact velocities of nanodroplets in practical applications are significantly higher than those of millimeter-sized droplets [40]; textured surfaces would be easier to be impaled by nanodroplets to trigger the Cassie-to-Wenzel wetting transition. A recent study [30] has demonstrated that the extrusion of liquid from asperities of pillared surfaces would dissipate a large amount of energy. Thus, because the significantly increased volume ratio of the liquid intruded into asperities to the nanodroplet would lead to extremely high viscous dissipation, the Wenzel-to-Cassie dewetting transition may be suppressed; as a result, impact outcomes and corresponding impact regimes would be altered as compared with millimeter-sized droplets. Moreover, several recent studies [56–59] have shown that the Cassie-to-Wenzel wetting transition for nanodroplets follows neither the sag mechanism nor the depinning mechanism, and an asymmetric wetting pathway was observed. This would further lead to different impact outcomes and regimes for nanodroplets.

In this study, the impact of nanodroplets on nanopillared surfaces is investigated via MD simulations, aiming to construct a comprehensive impact phase diagram. With constant intrinsic wettability, the pillar height is continuously increased to ensure that the surfaces cover Wenzel surfaces, coexisting Cassie–Wenzel surfaces, and Cassie surfaces. Various impact regimes and their boundaries are identified on these surfaces by changing impact velocities. The differences in impact regimes between the nanoscale and macroscale are analyzed and underlying mechanisms are discussed. Finally, a theoretical model is proposed to predict the critical velocity to trigger the Cassie-to-Wenzel wetting transition for impacting nanodroplets.

II. SIMULATION METHOD

The schematic of the initial configuration of the simulated system is shown in Fig. 2(a). The computational domain has dimensions of $24.53 \times 24.53 \times 25\,\text{nm}^3$ in the x-, y-, and z directions. Periodic boundary conditions are applied in the x- and y directions, and a nonperiodic and fixed boundary condition with a reflecting wall is set in the z direction to prevent loss of atoms. The simulated system consists of a water nanodroplet and a nanopillared platinum surface. Initially, the nanodroplet and the nanopillared surface are both generated by face-centered cubic crystals at a temperature of $T_0 = 300\,\text{K}$. The lattice constant for the nanopillared surface is set the same as the real platinum, $a_{\text{Pt}} = 3.9242\,\text{Å}$, and the interlayer distance of Pt atoms is $L = a_{\text{Pt}}/2$. The nanopillared surface consists of a flat substrate and square pillars that are perpendicular to the substrate. The flat substrate is extended to the borders of the computational domain in the x- and y directions and has a thickness of $7L$ in the z direction. The square pillars are regularly distributed on the flat substrate, whose height and width are denoted by h and w, respectively, with a pitch of p, as shown in Fig. 2(b). The values of h are changed to obtain Wenzel surfaces, coexisting Cassie–Wenzel surfaces, and Cassie surfaces. All the Pt atoms are fixed in their initial positions by spring forces during the whole simulation to ensure the rigidity of the nanopillared surface. In our simulations,

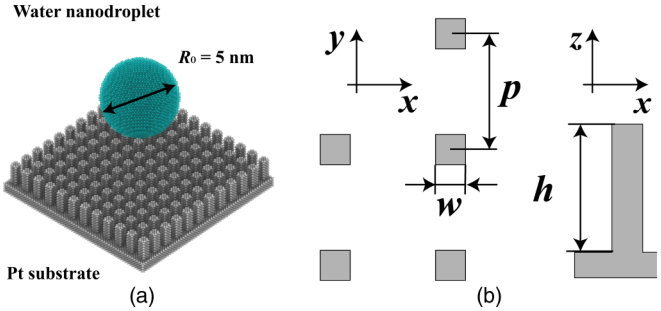

FIG. 2. (a) Schematic of the initial configuration of the simulated system and (b) structural parameters of nanopillars.

the initial radius of nanodroplets ranges from 3 to 10 nm. Once the initial radius is first specified, the water molecule number can be calculated by the liquid density (300 K) and volume. For example, a water nanodroplet with 5-nm radius contains 17 510 water molecules. The water nanodroplet is initially placed above the Pt surface with the spacing of at least 5 nm to avoid interactions between Pt atoms and water molecules during the relaxation.

The coarse-grained water model (mW) [60] is employed to model the interactions of water molecules. This model has been proven to accurately reproduce the surface tension, density, energetics, and structure of water. Moreover, the mW model shows higher computational efficiency as compared with other water models such as the four-site transferable intermolecular potential model (TIP4P) and the extended simple point charge model (SPC/E). The density and surface tension of water predicted by the mW model at 300 K are $\rho = 0.997\,\mathrm{g\,cm^{-3}}$ and $\gamma = 66\,\mathrm{mJ\,m^{-2}}$, respectively, which are very close to the real values. Based on these values, the Weber number, $We = \rho V_0^2 R_0/\gamma$, describing the ratio of inertial to capillary forces, is calculated. Here, V_0 is the impact velocity.

The interactions between the Pt-Pt and the Pt-water are described by the Lennard-Jones 12-6 potential, expressed by

$$U(r) = 4\varepsilon\left[\left(\frac{\sigma}{r}\right)^{12} - \left(\frac{\sigma}{r}\right)^{6}\right], \tag{1}$$

where ε is the depth of the potential wall, r is the distance between particles, and σ is the distance when the potential equals zero. The constant values of $\sigma_{\text{Pt-Pt}} = 2.47\times10^{-10}$ m, $\sigma_{\text{Water-Pt}} = 2.82\times10^{-10}$ m, and $\varepsilon_{\text{Pt-Pt}} = 0.4095$ eV are chosen. For the impact on structured surfaces, the effects of surfaces on impact are reflected in the intrinsic contact angle and structural parameters. Therefore, the values of $\varepsilon_{\text{Water-Pt}}$ are adjusted to obtain various intrinsic wettability of the platinum surface, which has been extensively adopted in previous MD studies [47–56].

The velocities and positions of particles are updated by the Velocity-Verlet algorithm with a time step of 0.002 ps. The canonical ensemble (*NVT*) with $T_0 = 300$ K is applied to the Pt surface in the whole simulation. The simulation can be divided into two stages. In the first stage, the center of mass of the droplet is fixed to its initial position, and the droplet is first relaxed for 300 000 time steps with the Nosé-Hoover thermostat in the *NVT* ensemble at 300 K and then is run in the microcanonical ensemble (*NVE*) for 200 000 time steps to achieve equilibrium. After that, an additional velocity component in the z direction, V_0, is imposed on all the water molecules in the nanodroplet, making the nanodroplet impact the nanopillared surface. The MD code is first validated by comparing the maximum spreading factor between the present and previous simulations for a water nanodroplet impacting smooth surfaces. As shown in Fig. S1 in the Supplemental Material [61], the present results are in good agreement with the previous simulations [47,49]. The validation is further implemented for the impact of a water nanodroplet on nanopillared surfaces. As shown in Fig. S2 [61], the simulated spreading factors on nanopillared surfaces agree well with previous results.

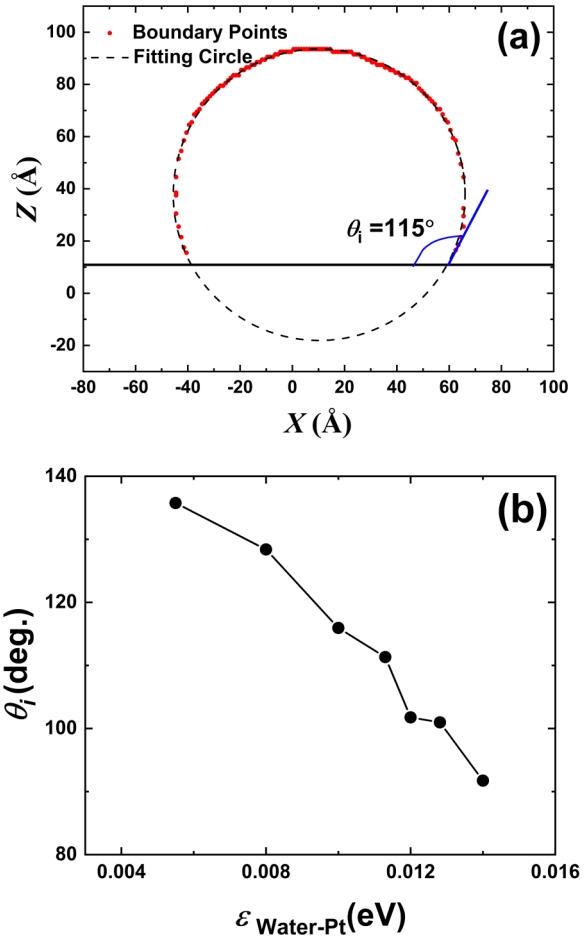

FIG. 3. Measurement of the intrinsic contact angle: (a) the circle fitting of the boundary of the water nanodroplet and (b) the intrinsic contact angles θ_i as a function of $\varepsilon_{\text{Water}-\text{Pt}}$.

III. RESULTS AND DISCUSSION

A. Intrinsic wettability

A series of MD simulations are performed to evaluate the intrinsic contact angles of the Pt surface at various values of $\varepsilon_{\text{Water-Pt}}$. The intrinsic contact angle is defined as the contact angle of an equilibrated water nanodroplet on a smooth surface. The boundary of the nanodroplet is defined as the isodensity line with a half density of liquid water at 300 K, as shown in Fig. S3 in the Supplemental Material [62]. The intrinsic contact angle is measured by a circle-fitting procedure of the boundary, as shown in Figs. 3(a) and S4 [63]. The dependence of the intrinsic contact angle on $\varepsilon_{\text{Water}-\text{Pt}}$ is shown in Fig. 3(b).

B. Impact regimes

The simulations are implemented with the fixed parameters of $w = 5L$, $p = 10L$, and $\theta_i = 116^\circ$ and the variable parameters of h ranging from $6L$ to $25L$ and We varying from 0.2 to 40.2 to obtain various impact outcomes. Higher Weber numbers are not considered here because our simulations indicate that no new impact regime occurs when We ranges from 40.2 to the splashing threshold.

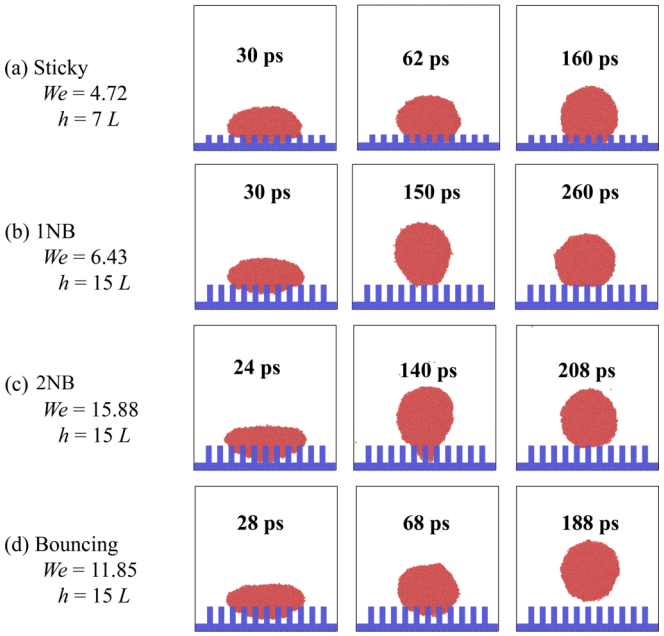

FIG. 4. Snapshots of impact outcomes for a nanodroplet impacting nanopillared surfaces: (a) sticky, (b) nonbouncing, (c) second nonbouncing, and (d) bouncing. The time when the nanodroplet just touches the surface is taken as $\tau = 0$. The surface properties are $w = 5L$, $p = 10L$, and $\theta_i = 116^\circ$.

Moreover, splashing has been well studied for both millimeter-sized [64] and nanoscale droplets [48,65], and hence, it is not involved in the present study. The snapshots of impact outcomes are shown in Fig. 4. Four kinds of outcomes are identified, i.e., sticky, 1NB, 2NB, and bouncing. The impact phase diagram is constructed in the *We*-*h* coordinate system, as shown in Fig. 5(a). For comparison, the same form of the phase diagram for millimeter-sized droplets is constructed based on theoretical models proposed by Bartolo *et al.* [14] and Deng *et al.* [21] and plotted in Fig. 5(b).

Except for the PPB regime, the other four regimes, i.e., sticky, 1NB, 2NB, and bouncing, which were found for the impact of millimeter-sized droplets, are observed for the impact of nanodroplets. However, the regime boundaries show significant differences, as shown in Figs. 5(a) and 5(b). In this section, the condition and feature of each impact regime will be described in detail, and the difference between the macroscale and nanoscale will be revealed.

On surfaces with pillar heights lower than $h_1 = 5.5L$, as shown in Fig. 4(a), the nanodroplet wets the bottom of the substrate and remains in the Wenzel state in the whole impact process regardless of *We*. The nanodroplet cannot bounce off the surface and eventually stays on the surface. Sticky is the only impact regime for $h < h_1$.

When pillar heights exceed h_1, a different outcome occurs. At higher *We,* the nanodroplet remains in the sticky regime, whereas at lower *We*, the nanodroplet does not wet the bottom of the substrate and remains in the Cassie state during the whole impact process, without bouncing off the surface, leading to the different regime of 1NB, as shown in Fig. 4(b). The nonbouncing in the 1NB regime can be attributed to the low initial kinetic energy of the nanodroplet at small *We*, which makes the nanodroplet neither intrude into gaps between nanopillars nor rebound from the surface. However, once the Cassie-to-Wenzel wetting transition is triggered at higher *We*, the liquid cannot dewet from the gaps, and finally, the nanodroplet stays in the Wenzel state without rebounding, falling into the sticky regime. Thus, the boundary between the two regimes is identified by the occurrence of the Cassie-to-Wenzel wetting transition.

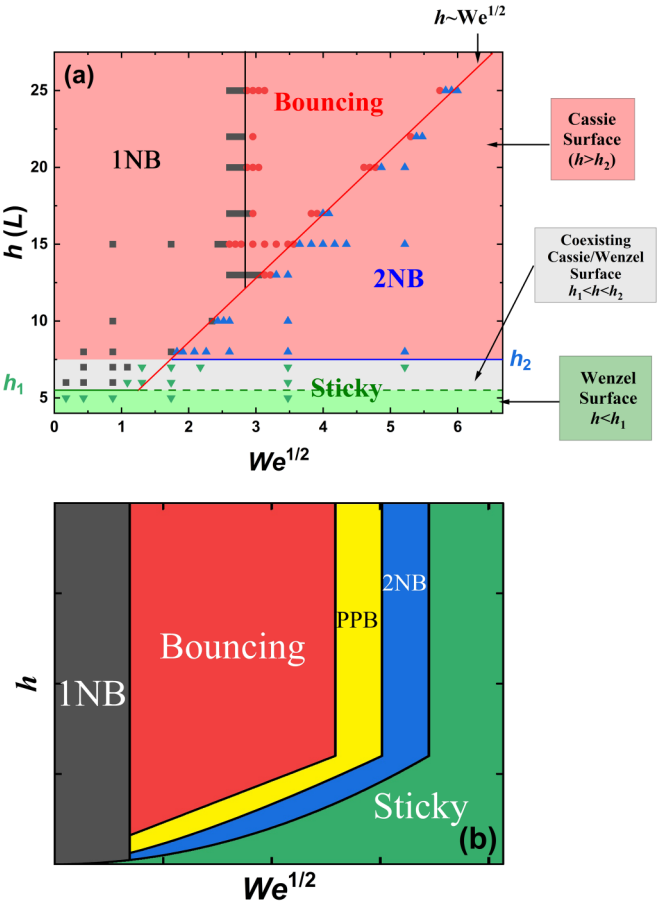

FIG. 5. Impact phase diagrams: (a) for the impact of nanodroplets and (b) for macroscale droplets. The surface properties employed in this work are $w = 5L$, $p = 10L$, and $\theta_i = 116^\circ$.

As pillar heights further increase and exceed $h_2 = 7.5L$, the sticky regime disappears but a different regime appears. Like in the cases with $h_1 < h < h_2$, nanodroplet is always in the Cassie state at low *We*, and finally stays on the surface without rebounding. When the impact velocity reaches a threshold, the central gaps beneath the nanodroplet are completely intruded by liquid, forming a partial wetting state (or mixed-wetting state). Subsequently, accompanied by the extrusion of liquid from the central gaps, the droplet returns to the Cassie state but does not bounce off the surface, leading to a different 2NB regime, as shown in Fig. 4(c). The difference between the 1NB and 2NB regimes lies in whether or not a partial wetting state is generated during the impact.

After pillar heights exceed $h_3 = 12.5L$, the 1NB and 2NB regimes still exist at low and high *We*, respectively, but a different bouncing regime is generated at moderate *We*. As shown in Fig. 4(d), in the bouncing regime, a small amount of liquid intrudes into the central gaps beneath the nanodroplet but does not touch the bottom of the substrate, and hence, neither the partial wetting state nor the Wenzel state is formed. After that, the intruding liquid extrudes from the central gaps so that the nanodroplet returns to the Cassie state and finally bounces off the surface. As shown in Fig. 5(a), there exist a lower limit and an upper limit of *We* to separate the bouncing regime from the 1NB regime and the 2NB regime, respectively. Intriguingly, the lower limit of *We* remains constant, whereas the upper limit increases with increasing the pillar height. Because the liquid only partially intrudes into the central gaps in both the 1NB and bouncing regimes, forming neither the partial

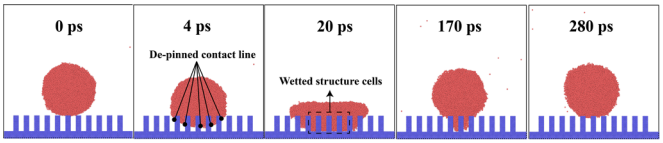

FIG. 6. Snapshots of an impacting nanodroplet in the 2NB regime at $We = 27.2$. The black dots denote the depinned contact line and the dashed rectangle shows the wetted gaps. The surface properties are $w = 5L$, $p = 10L$, and $\theta_i = 116^\circ$.

wetting state nor the Wenzel state, the transition from the 1NB regime to the bouncing regime would not depend on the wetting transition, and hence, the lower limit of *We* is independent of the pillar height. The transition from the 1NB regime to the bouncing regime is similar to that on smooth substrates, which has been well investigated in previous studies [66,67]. On the contrary, the difference between the bouncing and 2NB regimes lies in whether or not the partial wetting state is generated so that taller pillars require higher *We* to achieve the partial wetting state. As a consequence, the upper limit of *We* strongly depends on the pillar height and monotonously increases with the pillar height.

Although the same four impact regimes are observed for the macroscale and the nanoscale impact, several significant differences between them can be distinguished by comparing Figs. 5(a) and 5(b). (1) The 2NB and sticky regimes can coexist on the same surface at different *We* for the macroscale impact, whereas they separately occur on the surfaces with taller and shorter pillars for the nanoscale impact. (2) The PPB regime is observed for the macroscale impact but not for the nanoscale impact. The partial wetting state is formed in the PPB regime for the macroscale impact; however, only a very small proportion of gaps beneath the center of the impacting droplet are completely wetted [17,21,29,30]. Because of the relatively low-energy dissipation generated by the liquid intrusion, there is still sufficient kinetic energy to lift the droplet to depart from the surface, with the intruding liquid remaining in the gaps [17,21]. Owing to small sizes, a larger proportion of gaps are completely intruded in the 2NB regime for the nanoscale impact. For example, as shown in Fig. 6, nearly half of the gaps beneath the nanodroplet are wetted. Both intrusion and extrusion of liquid need to overcome energy barriers [56]; thus, the intrusion into and the extrusion from the larger proportion of gaps would dissipate an enormous amount of energy. Furthermore, recent studies [47,49,51,53,55] have shown that the viscous dissipation in the bulk nanodroplet is significantly enhanced at the nanoscale. As a result of the two special energy dissipation mechanisms, once the partial wetting state is generated for the nanoscale impact, the nanodroplet can only return to the Cassie state but cannot bounce off the surface. Thus, the PPB regime cannot be observed for the nanoscale impact. It is worth noting that dissipation can also arise from contact-line friction. However, this dissipation is relatively insignificant on nanostructured superhydrophobic surfaces, as compared to the viscous dissipation in the bulk nanodroplet. (3) According to the theoretical model proposed by Bartolo *et al.* [14], when the depinning mechanism dominates the wetting transition, the critical impact velocity for the wetting transition remains constant, independent of the pillar height. Therefore, the critical *We* separating the bouncing regime from the PPB regime and the critical *We* separating the 2NB regime from the sticky regime at relatively taller pillars both remain constant. As shown in Fig. 6, depinning of the contact line is observed in the 2NB regime for the impact of nanodroplets; however, the critical *We* between the bouncing and 2NB regimes does not remain constant but increases with the pillar height, which is contradictory to the theoretical model of Bartolo *et al.* [14].

C. Wetting states

The enhanced viscous effect and the altered viscous dissipation mechanism at the nanoscale are two potential reasons for different impact regimes between the macroscale and nanoscale impact.

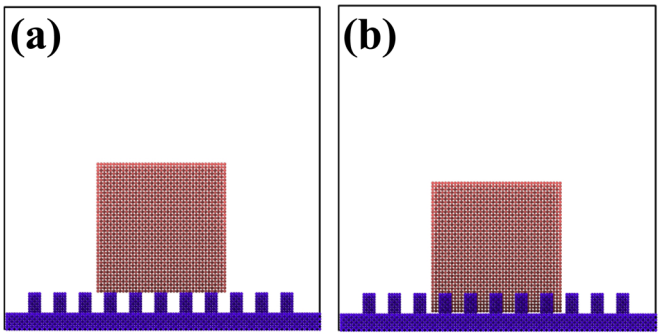

FIG. 7. Schematics of the simulation systems with the initial wetting state of a nanodroplet being (a) the Cassie state and (b) the Wenzel state.

Moreover, wetting states may also contribute to this difference. This speculation can be initially verified by the following fact. It was reported that the 2NB regime and sticky regimes could coexist on one textured surface by increasing impact velocities for the macroscale impact [17,21,22,29,30]. However, this coexistence merely occurs on a coexisting Cassie–Wenzel surface, never on a Cassie or a Wenzel surface. On a Cassie surface, the Cassie state is the globally energetic minimum state, and hence, the final droplet is never in the Wenzel state. Likewise, the final droplet on a Wenzel surface is never in the Cassie state. Therefore, the 2NB regime and sticky regimes are impossible to coexist on a Cassie or a Wenzel surface. Recent experiments [39,68] also demonstrated that the impact of milliliter-sized droplets on a monostable Cassie surface shows different impact regimes from those on a coexisting Cassie–Wenzel surface, i.e., the sticky regime disappears and a different bouncing regime with the Cassie-Wenzel-Cassie wetting transition is observed. This result supports that impact regimes depend on wetting states of textured surfaces. Based on this fact, the dependence of wetting states on pillar heights is studied in this section.

The wetting states of a water nanodroplet on a nanopillared surface with various intrinsic contact angles were identified by Chen *et al.* [69]. They found that the surface is the Wenzel surface, the coexisting Cassie–Wenzel surface, and the Cassie surface successively as the intrinsic contact angle increases. Our MD simulations reproduce this result, as shown in Fig. S5 in the Supplemental Material [70]. Previous studies [25,69] have shown that the three kinds of surfaces can also be realized by an increase in pillar heights. A series of simulations are performed to investigate the equilibrium wetting states of a nanodroplet on nanopillared surfaces with various pillar heights. The simulation method is similar to that adopted in Ref. [69]. On each nanopillared surface, two initial wetting states of a water nanodroplet are specified, i.e., the Wenzel state and the Cassie state, as shown in Fig. 7. In all the simulations, the following parameters are fixed: $w = 5L$, $p = 10L$, and $\theta_i = 116^\circ$; only the pillar height is changed. The initial configuration of the nanodroplet is a water cube with side lengths of 10 nm. The system is relaxed in the *NVT* ensemble at $T_0 = 300\,\mathrm{K}$. When the center of mass of the nanodroplet keeps stable in the z direction, the nanodroplet is considered to achieve equilibrium.

As shown in Fig. 8, when pillar heights are smaller than $h_1 = 5.5L$, the equilibrated nanodroplet is always in the Wenzel state no matter what the initial wetting state is. On the contrary, when pillar heights are larger than $h_2 = 7.5L$, the equilibrated nanodroplet stays in the Cassie state. Between the two critical pillar heights, the wetting state of the equilibrated nanodroplet is identical to the initial wetting state. This result indicates that the surfaces are the Wenzel surfaces at $h < h_1$, the coexisting Cassie–Wenzel surfaces at $h_1 < h < h_2$, and the Wenzel surfaces at $h > h_2$.

Based on this result, the phase diagram shown in Fig. 5(a) can be divided into three regions. At $h < h_1$, the surfaces are the Wenzel surfaces; the Wenzel state is the globally energetic minimum state. When a nanodroplet impacts such surfaces, the Cassie-to-Wenzel wetting transition must be

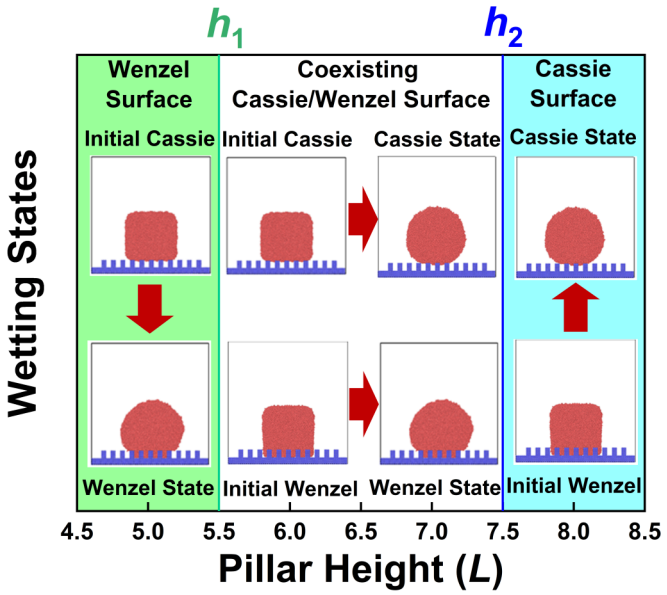

FIG. 8. The equilibrium wetting states of a nanodroplet on nanopillared surfaces with various pillar heights. The surface properties are $w = 5L$, $p = 10L$, and $\theta_i = 116^\circ$.

triggered. However, the high viscous dissipation during the impact and the large energy barrier for the Wenzel-to-Cassie dewetting transition prevent the occurrence of the dewetting transition so that the nanodroplet keeps in the Wenzel state, forming the only sticky regime. At $h_1 < h < h_2$, the surfaces are the coexisting Cassie–Wenzel surfaces; the Cassie and Wenzel state can coexist on one texture surface. The Cassie-to-Wenzel wetting transition cannot be triggered at small impact velocities. Meanwhile, there is no sufficient kinetic energy to make the nanodroplet rebound from the surface; the nanodroplet, therefore, stays on the surface, keeping in the Cassie state, forming the 1NB regime. The Cassie-to-Wenzel wetting transition is triggered at high impact velocities, which dissipates an enormous amount of energy. On the other hand, viscous dissipation in the bulk nanodroplet also increases significantly at high impact velocities [51]. As a result, the nanodroplet has no enough energy to realize the dewetting transition, forming the sticky regime. Therefore, only two regimes are observed on the coexisting surfaces. At $h > h_2$, the surfaces are the Cassie surfaces with the globally energetic minimum Cassie state. On such surfaces, only the 1NB and 2NB regimes occur when $h_2 < h < 12.5L$, or the 1NB, bouncing, and 2NB regimes all occur at $h > 12.5L$. The occurrence of the 1NB regime at small impact velocities is similar to that on the coexisting surfaces. As impact velocities further increase, the 1NB regime transition to the 2NB regime at $h_2 < h < 12.5L$. This can be explained as follows. The large impact velocities induce the formation of a partial wetting state, which dissipates a part of kinetic energy. Moreover, there is very high viscous dissipation in the bulk nanodroplet during the impact. Thus, although the dewetting transition follows a barrierless energy pathway, there is still not enough energy to make the nanodroplet rebound from the surface, and hence, the nanodroplet finally returns to the Cassie state without bouncing. Because the Cassie state has lower energy for the surfaces with pillar heights larger than $12.5L$, the partial wetting state is not generated at the same impact velocities as shorter pillar heights ($h_2 < h < 12.5L$). In other words, the liquid does not touch the bottom of the substrate with a small energy loss. But, at the same time, high impact velocities ensure enough residual kinetic energy to lift the nanodroplet; therefore, the bouncing regime is initiated. When impact velocities further increase, the partial wetting state generates; the bouncing regime transitions to the 2NB regime.

To examine the effects of intrinsic surface wettability on impact outcomes, the impact of a water nanodroplet on nanopillared surfaces with intrinsic contact angles of $\theta_i = 92^\circ$, 111°, and 128° at the same $We = 11.85$ is additionally stimulated. The structural parameters are the same as those in Fig. 5(a). As shown in Fig. S6 in the Supplemental Material [71], the outcome is sticky for $\theta_i = 92^\circ$, 2NB for $\theta_i = 111^\circ$, and bouncing for 2NB for $\theta_i = 128^\circ$. The bouncing is suppressed when the surface becomes more hydrophilic, and hence, impact phase diagrams would be altered for intrinsically hydrophilic surfaces. However, as mentioned before, the occurrence of various impact regimes depends actually on the wetting states of textured surfaces. As shown in Fig. S5 in the Supplemental Material [70], with the fixed structural parameters, the Wenzel surface, coexisting Cassie–Wenzel surface, and Cassie surface can be obtained in sequence by increasing θ_i. Thus, the effects of θ_i on impact regimes are similar to the effects of pillar height. Therefore, it is reasonably expected that when the intrinsic contact angle is small enough, textured surfaces belong to the Wenzel surface; only the sticky regime can be observed. When gradually increasing the intrinsic contact angle, texture surfaces would first convert to the coexisting Cassie–Wenzel surface and then to the Cassie surface, so the 1NB, bouncing, and 2NB regime would occur but the sticky regime would disappear.

D. Criterion for wetting transition at the nanoscale

The 2NB regime takes place on the coexisting Cassie–Wenzel surface for the macroscale impact, whereas it is observed only on the monostable Cassie surface for the nanoscale impact. The 2NB regime is related to the occurrence of the wetting transition. Therefore, the difference in the 2NB may imply different wetting transition mechanisms for the two scales. In this section, the criterion for wetting transition at the nanoscale is discussed.

Two kinds of mechanisms of wetting transition were proposed by Bartolo *et al.* [14]. In the sag mechanism, the contact line is pinned at the corners of pillars, whereas depinning of the contact line occurs in the depinning mechanism. In our simulations, depinning is also observed, as shown in Fig. 6, and hence, the depinning mechanism is first examined for the wetting transition at the nanoscale. According to the theoretical model of Bartolo *et al.* [14], the critical velocity, $V_{\rm cr}$, to trigger the wetting transition in the depinning mechanism is equal to the critical velocity of depinning and thereby is independent of pillar heights. Several additional simulations are performed for a water nanodroplet impacting nanopillared surfaces with various structural properties and intrinsic contact angles to extract $V_{\rm cr}$. The critical Weber numbers, $We_{\rm cr} = \rho V_{\rm cr}^2 R_0/\gamma$, at various pillar heights are plotted in Fig. 9. A relationship of $We_{\rm cr}^{1/2} \sim h$ is yielded, indicating that the model of Bartolo *et al.* [14] is invalid at the nanoscale.

A possible reason for the model failure is comparable sizes of nanodroplets and nanostructures. After impacting a pillared surface, a droplet spreads over and deforms on the surface. At the same time, if the wetting transition is triggered, like the motion of menisci through pores [72], the contact line would move downward pillar sidewalls. The timescales for the deformation and the contact line movement on sidewalls can be estimated as R_0/V_0 and h/V_0, respectively. At the macroscale, the droplet volume is much larger than the volume of gaps intruded by the liquid [14–22], and hence, the ratio of the two timescales, R_0/h, is commonly larger than 20. This estimation implies that the effect of deformation on the contact line movement on pillar sidewalls can be neglected so that the dynamic pressure that depends on the impact velocity remains constant during the wetting transition. On the contrary, the timescale ratio, R_0/h, significantly reduces at the nanoscale, leading to a non-negligible effect of the droplet deformation during the wetting transition, as shown in Fig. 10. Because of the deformation, the dynamic pressure rapidly decreases during the conversion from kinetic energy to surface energy, causing the reduced movement velocity of the contact line on pillar sidewalls. Therefore, even if the contact line is depinned, it may stop before the bottom of the substrate is wetted. The assumption that the wetting transition would take place once the depinning is triggered fails at the nanoscale so that the model of Bartolo *et al.* [14] is no longer suitable for the impact of nanodroplets.

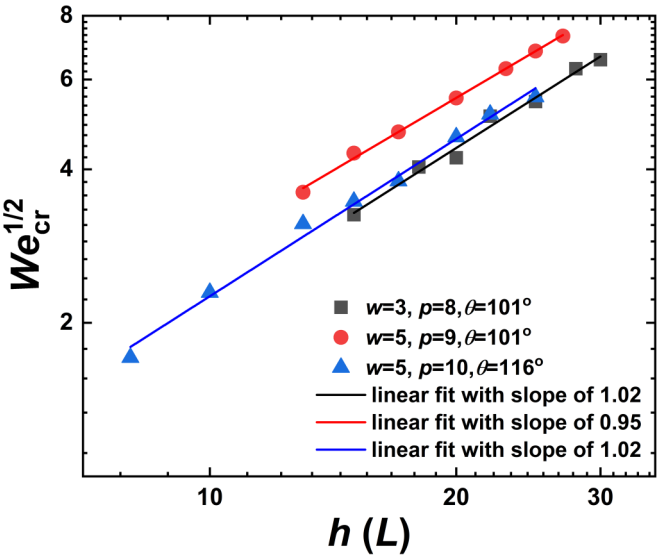

FIG. 9. The dependence of the critical Weber number on the pillar height.

E. Critical impact velocity

To predict the critical velocity for triggering the wetting transition at the nanoscale, a theoretical model is developed based on the analysis of dynamic behaviors of impacting nanodroplets. Assuming that the contact line is initially pinned at the corners of nanopillars, the vertical component of capillary force at one nanopillar can be calculated by [14]

$$F_c = 4\gamma w \cos\theta_i. \tag{2}$$

The capillary force is considered as a resistance force to hinder the contact line movement along the sidewalls of the pillar. Hence, the deceleration of the contact line can be estimated as $a_{\mathrm{cl}} \sim F_c/\rho\Omega_a$, where $\Omega_a = \Omega_0/N_p$ represents the average liquid volume per nanopillar, $\Omega_0 = 4\pi R_0^3/3$ is the nanodroplet volume, and N_p is the number of nanopillars covered by the nanodroplet, which can be calculated by $N_p = \pi R_{\mathrm{s}}^2/p^2$, with R_{s} being the spreading radius of the nanodroplet. Thus, a_{cl} can scale as follows:

$$a_{\mathrm{cl}} \sim \frac{\gamma w \cos\theta_i}{\rho p^2 R_0^3} R_s^2 \tag{3}$$

Because only the spreading radius R_s is a function of time, the average deceleration, a_{cla}, of the contact line can be expressed as

$$a_{\mathrm{cla}} \sim \frac{\gamma w \cos\theta_i}{\rho p^2 R_0^3} R_{\mathrm{sa}}^2, \tag{4}$$

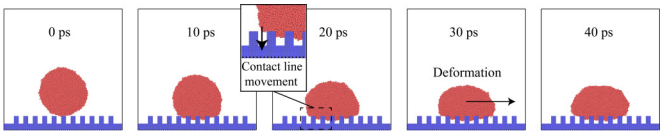

FIG. 10. Deformation of the nanodroplet and the movement of the contact line on the sidewalls of pillars. As the contact line moves downward, the nanodroplet shows significant deformation.

where R_{sa}^2 denotes the mean of the square of spreading radius during the wetting transition. To obtain the scaling law of the average deceleration, the scaling law of R_{sa} should be figured out. The spreading kinetics of impacting nanodroplets in the early spreading stage was studied by Kobayashi *et al.* [73]. They found that the temporal revolution of the spreading radius of nanodroplets in the early spreading stage can be described as $R_s/R_0 \sim (\tau_s V_0/D_0)^{1/2}$, where τ_s denotes the spreading time. Zhang *et al.* [74] demonstrated the applicability of this scaling law in the kinematic stage of impacting droplets on textured surfaces with a large liquid volume penetrating the surface asperities. Therefore, the mean of the square of spreading radius during the wetting transition can scale as

$$R_{sa}^2 = \frac{1}{\tau_{cls}} \int_0^{\tau_{cls}} R_s^2 d\tau \sim \frac{R_0}{4} V_0 \tau_{cls}, \tag{5}$$

where τ_{cls} denotes the length of time from the contact line starting depinning to stopping moving. Our simulations show that τ_{cls} remains almost constant regardless of the impact velocity and pillar height. The movement of the contact line on sidewalls of pillars occurs in the early spreading stage, and hence, it can be reasonably assumed that only inertial and capillary forces dominate during this period. As a result, the constant τ_{cls} can scale as the inertial-capillary time, $\tau_{cls} \sim (\rho R_0^3/\gamma)^{1/2}$. Thus, Eq. (4) can be rearranged as

$$a_{cla} \sim \frac{\gamma w \cos\theta_i}{\rho p^2 R_0} We^{1/2}. \tag{6}$$

The maximum displacement of the contact line on sidewalls of pillars can be estimated as $\Delta Z \sim -V_0^2/a_{cla}$ since the velocity of the contact line decreases from V_0 to zero. If $\Delta Z = h$, the contact line can touch the bottom of the substrate, leading to the occurrence of a partial wetting state. The corresponding minimum impact velocity is the critical velocity, expressed as

$$h \sim -\frac{V_{cr}^2}{a_{cla}}. \tag{7}$$

Combining Eqs. (6) and (7) yields

$$We_{cr}^{1/2} \sim -\frac{wh\cos\theta_i}{p^2} = -h^* \cos\theta_i, \tag{8}$$

where $h^* = wh/p^2$ is defined as the dimensionless pillar height, describing the structural property of a nanopillared surface.

Equation (8) represents the critical impact velocity for triggering the wetting transition, at which a partial wetting state or the Wenzel state is generated. Accordingly, it is expected that Eq. (8) can describe the boundary between the 1NB and sticky regimes on the coexisting Cassie–Wenzel surfaces, and the boundary between the 1NB and 2NB regimes on the Cassie surface, and the boundary between the bouncing and 2NB regimes on the Cassie surface. This expectation is well verified in Fig. 5(a). However, it should be noted that the phase diagram in Fig. 5(a) is obtained only at the fixed parameters of $w = 5L$, $p = 10L$, and $\theta_i = 116^\circ$ so further verification is necessary. A series of additional MD simulations are performed on the surfaces with various structural parameters and intrinsic contact angles. The critical impact velocities for triggering the wetting transition are determined by simulations. As shown in Figs. 11(a) and 11(b), the scaling laws $We_{cr}^{1/2} \sim h^*$ and $We_{cr}^{1/2} \sim -\cos\theta_i$ are verified. Additionally, the critical Weber numbers are also extracted from MD simulations for nanodroplets with various initial radii to examine the robustness of MD results to the droplet size. As shown in Fig. 11(c), We_{cr} for various nanodroplet initial radii remains constant, which is in good agreement with the model prediction.

It can be seen that the boundary between the 1NB and bouncing regimes on the coexisting Cassie–Wenzel surfaces slightly deviates from Eq. (8). This deviation is explained as follows. As shown in Fig. 12, the liquid-air interface in the gaps is a meniscus instead of a plane. The meniscus would first come into contact with the bottom of the substrate; however, it is assumed to be the

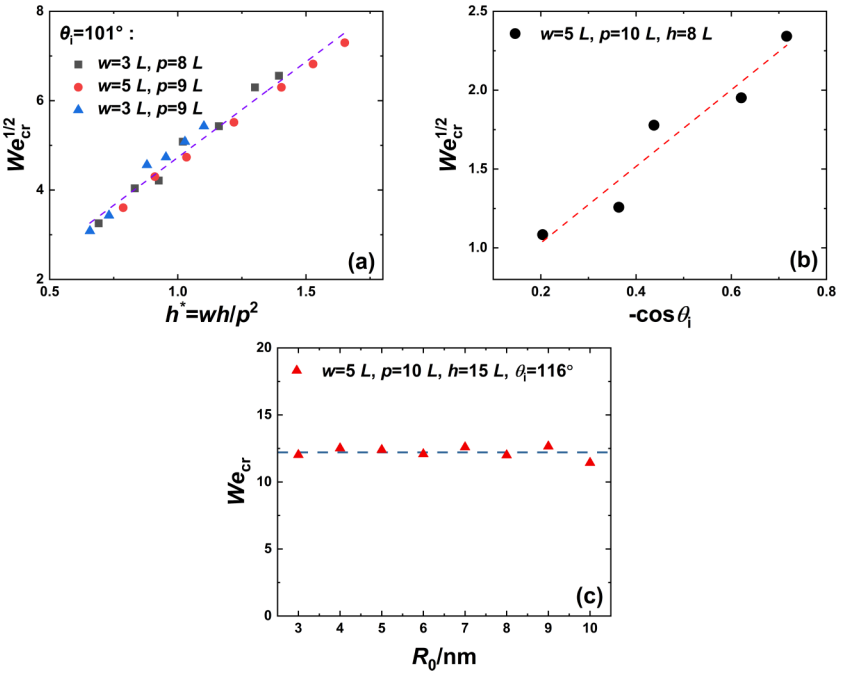

FIG. 11. Validation of the critical impact velocity on the nanopillared surfaces with (a) various structural parameters, (b) various intrinsic contact angles, and (c) various initial droplet radii. The dotted lines are predicted by the model, and the symbols are simulated by MD simulations.

contact line in the present model. The height, h_{m}, of the meniscus can be calculated by

$$h_m = \frac{\sin\theta_i - 1}{2\cos\theta_i} l_{\mathrm{gap}}, \tag{9}$$

where l_{gap} is the gap width between two adjacent pillars. The maximum gap width is $l_{\mathrm{gap}} = 2^{0.5}(p-w)$ for the present nanopillared surfaces. Thus, when the meniscus touches the bottom of the substrate, the maximum displacement of the contact line should be modified as $\Delta Z = h - h_{\mathrm{m}}$,

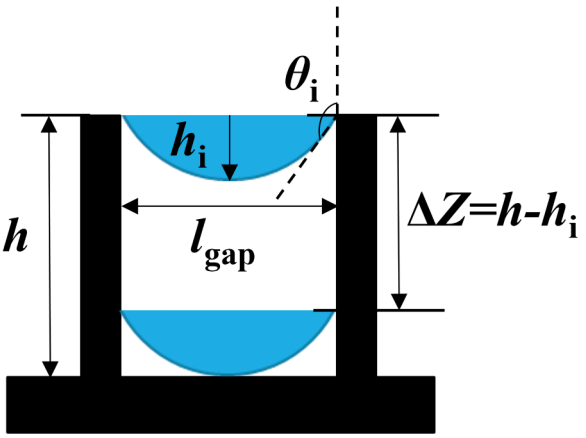

FIG. 12. The schematic of the meniscus between pillars.

and Eq. (8) should be changed as

$$We_{\mathrm{cr}}^{1/2} \sim -\frac{w(h-h_m)\cos\theta_i}{p^2}. \tag{10}$$

The value of h_{m} is estimated for the surfaces employed in the phase diagram. With the parameter values of $w = 5L$, $p = 10L$, and $\theta_i = 116^\circ$, h_{m} is 0.82 L. The pillar height ranges from $5.5L$ to $7.5L$ for the coexisting Cassie–Wenzel surfaces employed in the phase diagram. As compared with Eq. (10), the critical Weber number predicted by Eq. (8) is overestimated by 38% at $h = 5.5L$ and by 26% at $h = 7.5L$.

Equation (10) can be rewritten as

$$V_{\mathrm{cr}} \sim -\frac{h^*\cos\theta_i\sqrt{\gamma/\rho}}{R_0^{1/2}}, \tag{11}$$

where h^* is modified as $h^* = w(h-h_{\mathrm{m}})/p^2$. According to Eq. (11), at the nanoscale, the critical impact velocity for triggering the wetting transition increases with a decrease in the droplet size. Moreover, it is expected that Eqs. (10) and (11) may also be applicable for microscale and macroscale impacting droplets as long as the feature size of microstructures is comparable to the droplet size.

IV. CONCLUSIONS

MD simulations are performed to investigate the impact of a water nanodroplet on nanopillared surfaces, aiming to construct a nanoscale impact phase diagram. Depending on pillar heights and impact Weber numbers, four impact regimes, including 1NB, bouncing, 2NB, and sticky regimes, are identified, which are compared with those observed at the macroscale to examine the scale effects. The main conclusions are as follows.

(1) With a fixed intrinsic contact angle, monostable Wenzel surfaces, metastable Cassie–Wenzel surfaces, and monostable Cassie surfaces are successively obtained by increasing pillar heights. On these surfaces, different impact regimes are identified. On the Wenzel surfaces ($h < 5.5L$), the equilibrated nanodroplet always remains in the Wenzel state and adheres to the surfaces regardless of impact Weber numbers, forming the only sticky regime. On the coexisting Cassie–Wenzel surfaces ($5.5L < h < 7.5L$), the 1NB regime is observed at low Weber numbers but it converts to the sticky regime at high Weber numbers. On the Cassie surfaces ($h > 7.5L$), the sticky regime is replaced by the 2NB, with the coexistence of the 1NB and 2NB regimes at $7.5L < h < 12.5L$, and the coexistence of the 1NB, bouncing, and 2NB regimes at $h > 12.5L$.

(2) Three differences in impact regimes between the nanoscale and macroscale are distinguished. First, the 2NB and sticky regimes can coexist on one surface at the macroscale, whereas they separately occur on the surfaces with taller and shorter pillars at the nanoscale. Second, the PPB regime is not observed at the nanoscale but does at the macroscale. Third, when depinning of the contact line takes place, the critical Weber number for the wetting transition remains constant at the macroscale; conversely, it strongly depends on pillar heights at the nanoscale.

(3) The transition from the 1NB to sticky regimes, from the 1NB to 2NB regimes, and from the bouncing to 2NB regimes are all associated with the formation of a partial wetting state. Because of comparable volumes of the nanodroplet and the gaps intruded by liquid, the wetting transition does not follow the depinning mechanism that is widely accepted at the macroscale. Considering this volume effect, a theoretical model is built to reveal the nanoscale wetting transition mechanism and thereby predict the critical Weber numbers for triggering the wetting transition. The prediction is in good agreement with the MD simulations, and hence, precisely captures the boundaries between the 1NB and sticky regimes, between the 1NB and 2NB regimes, and between the bouncing and 2NB regimes.

ACKNOWLEDGMENTS

This study was partially supported by the State Key Program of National Natural Science Foundation of China (Grant No. 51936004), Science Fund for Creative Research Groups of the National Natural Science Foundation of China (Grant No. 51821004), and the Fundamental Research Funds for the Central Universities (Grant No. 2020MS063).

[1] Y. Liu, X. Li, J. Jin, J. Liu, Y. Yan, Z. Han, and L. Ren, Anti-icing property of bio-inspired micro-structure superhydrophobic surfaces and heat transfer model, Appl. Surf. Sci. **400**, 498 (2017).
[2] R. Dou, J. Chen, Y. Zhang, X. Wang, D. Cui, Y. Song, L. Jiang, and J. Wang, Anti-icing coating with an aqueous lubricating layer, ACS Appl. Mater. Interfaces **6**, 6998 (2014).
[3] A. Nakajima, K. Hashimoto, T. Watanabe, K. Takai, G. Yamauchi, and A. Fujishima, Transparent superhydrophobic thin films with self-cleaning properties, Langmuir **16**, 7044 (2000).
[4] B. Bhushan, Y. C. Jung, and K. Koch, Micro-, nano-and hierarchical structures for superhydrophobicity, self-cleaning and low adhesion, Philos. Trans. R. Soc. A **367**, 1631 (2009).
[5] C. Hao, Y. Liu, X. Chen, J. Li, M. Zhang, Y. Zhao, and Z. Wang, Bioinspired interfacial materials with enhanced drop mobility: From fundamentals to multifunctional applications, Small **12**, 1825 (2016).
[6] J. Wang, Z. Zheng, H. Li, W. Huck, and H. Sirringhaus, Dewetting of conducting polymer inkjet droplets on patterned surfaces, Nat. Mater. **3**, 171 (2004).
[7] H. T. Yudistira, V. D. Nguyen, P. Dutta, and D. Byun, Flight behavior of charged droplets in electrohydrodynamic inkjet printing, Appl. Phys. Lett. **96**, 023503 (2010).
[8] B. M. Pikkula, J. H. Torres, J. W. Tunnell, and B. Anvari, Cryogen spray cooling: Effects of droplet size and spray density on heat removal, Lasers Surg. Med. **28**, 103 (2001).
[9] E. A. Silk, E. L. Golliher, and R. P. Selvam, Spray cooling heat transfer: Technology overview and assessment of future challenges for micro-gravity application, Energy Convers. Manage. **49**, 453 (2008).
[10] A. Lafuma and D. Quéré, Superhydrophobic states, Nat. Mater. **2**, 457 (2003).
[11] S. Wang, K. Liu, X. Yao, and L. Jiang, Bioinspired surfaces with superwettability: New insight on theory, design, and applications, Chem. Rev. **115**, 8230 (2015).
[12] S. Zhang, J. Huang, Y. Cheng, H. Yang, Z. Chen, and Y. Lai, Bioinspired surfaces with superwettability for anti-icing and ice-phobic application: Concept, mechanism, and design, Small **13**, 1701867 (2017).
[13] S. Nishimoto and B. Bhushan, Bioinspired self-cleaning surfaces with superhydrophobicity, superoleophobicity, and superhydrophilicity, RSC Adv. **3**, 671 (2013).
[14] D. Bartolo, F. Bouamrirene, E. Verneuil, A. Buguin, P. Silberzan, and S. Moulinet, Bouncing or sticky droplets: Impalement transitions on superhydrophobic micropatterned surfaces, EPL **74**, 299 (2006).
[15] M. Reyssat, A. Pépin, F. Marty, Y. Chen, and D. Quéré, Bouncing transitions on microtextured materials, EPL **74**, 306 (2006).
[16] Z. Wang, C. Lopez, A. Hirsa, and N. Koratkar, Impact dynamics and rebound of water droplets on superhydrophobic carbon nanotube arrays, Appl. Phys. Lett. **91**, 023105 (2007).
[17] D. Hee Kwon and S. Joon Lee, Impact and wetting behaviors of impinging microdroplets on superhydrophobic textured surfaces, Appl. Phys. Lett. **100**, 171601 (2012).
[18] C. Lee, Y. Nam, H. Lastakowski, J. I. Hur, S. Shin, A.-L. Biance, C. Pirat, and C. Ybert, Two types of Cassie-to-Wenzel wetting transitions on superhydrophobic surfaces during drop impact, Soft Matter **11**, 4592 (2015).
[19] Y. C. Jung and B. Bhushan, Dynamic effects of bouncing water droplets on superhydrophobic surfaces, Langmuir **24**, 6262 (2008).
[20] H.-M. Kwon, A. T. Paxson, K. K. Varanasi, and N. A. Patankar, Rapid Deceleration-Driven Wetting Transition During Pendant Drop Deposition on Superhydrophobic Surfaces, Phys. Rev. Lett. **106**, 036102 (2011).
[21] T. Deng, K. K. Varanasi, M. Hsu, N. Bhate, C. Keimel, J. Stein, and M. Blohm, Nonwetting of impinging droplets on textured surfaces, Appl. Phys. Lett. **94**, 133109 (2009).

[22] N. D. Patil, R. Bhardwaj, and A. Sharma, Droplet impact dynamics on micropillared hydrophobic surfaces, Exp. Therm Fluid Sci. **74**, 195 (2016).
[23] V. Vaikuntanathan and D. Sivakumar, Transition from Cassie to impaled state during drop impact on groove-textured solid surfaces, Soft Matter **10**, 2991 (2014).
[24] E. Bormashenko, Progress in understanding wetting transitions on rough surfaces, Adv. Colloid Interface Sci. **222**, 92 (2015).
[25] N. A. Patankar, Transition between superhydrophobic states on rough surfaces, Langmuir **20**, 7097 (2004).
[26] B. He, N. A. Patankar, and J. Lee, Multiple equilibrium droplet shapes and design criterion for rough hydrophobic surfaces, Langmuir **19**, 4999 (2003).
[27] N. A. Patankar, Consolidation of hydrophobic transition criteria by using an approximate energy minimization approach, Langmuir **26**, 8941 (2010).
[28] E. Bormashenko, A. Musin, G. Whyman, and M. Zinigrad, Wetting transitions and depinning of the triple line, Langmuir **28**, 3460 (2012).
[29] J. Hyväluoma and J. Timonen, Impalement transitions in droplets impacting microstructured superhydrophobic surfaces, Europhys. Lett. **83**, 64002 (2008).
[30] J. Hyväluoma and J. Timonen, Impact states and energy dissipation in bouncing and non-bouncing droplets, J. Stat. Mech. (2009) P06010.
[31] T. Koishi, K. Yasuoka, S. Fujikawa, T. Ebisuzaki, and X. C. Zeng, Coexistence and transition between Cassie and Wenzel state on pillared hydrophobic surface, Proc. Natl. Acad. Sci. USA **106**, 8435 (2009).
[32] T. Koishi, K. Yasuoka, and X. C. Zeng, Molecular dynamics simulation of water nanodroplet bounce back from flat and nanopillared surface, Langmuir **33**, 10184 (2017).
[33] A. Cassie and S. Baxter, Wettability of porous surfaces, Trans. Faraday Soc. **40**, 546 (1944).
[34] R. N. Wenzel, Resistance of solid surfaces to wetting by water, Ind. Eng. Chem. **28**, 988 (1936).
[35] M. Nosonovsky and B. Bhushan, Patterned nonadhesive surfaces: Superhydrophobicity and wetting regime transitions, Langmuir **24**, 1525 (2008).
[36] P. Papadopoulos, L. Mammen, X. Deng, D. Vollmer, and H.-J. Butt, How superhydrophobicity breaks down, Proc. Natl. Acad. Sci. USA **110**, 3254 (2013).
[37] J. Oh, G. Manukyan, D. Van den Ende, and F. Mugele, Electric-field–driven instabilities on superhydrophobic surfaces, Europhys. Lett. **93**, 56001 (2011).
[38] E. Bormashenko, R. Pogreb, G. Whyman, Y. Bormashenko, and M. Erlich, Vibration-induced Cassie-Wenzel wetting transition on rough surfaces, Appl. Phys. Lett. **90**, 201917 (2007).
[39] S. Shi, C. Lv, and Q. Zheng, Drop impact on two-tier monostable superrepellent surfaces, ACS Appl. Mater. Interfaces **11**, 43698 (2019).
[40] P. Galliker, J. Schneider, H. Eghlidi, S. Kress, V. Sandoghdar, and D. Poulikakos, Direct printing of nanostructures by electrostatic autofocussing of ink nanodroplets, Nat. Commun. **3**, 890 (2012).
[41] Q. An, S.-N. Luo, W. A. Goddard III, W. Han, B. Arman, and W. L. Johnson, Synthesis of single-component metallic glasses by thermal spray of nanodroplets on amorphous substrates, Appl. Phys. Lett. **100**, 041909 (2012).
[42] M. Gamero-Castaño, A. Torrents, R. Borrajo-Pelaez, and J.-G. Zheng, Amorphization of hard crystalline materials by electrosprayed nanodroplet impact, J. Appl. Phys. **116**, 174309 (2014).
[43] A. S. Rana, D. A. Lockerby, and J. E. Sprittles, Lifetime of a Nanodroplet: Kinetic Effects and Regime Transitions, Phys. Rev. Lett. **123**, 154501 (2019).
[44] S. Perumanath, M. K. Borg, J. E. Sprittles, and R. Enright, Molecular physics of jumping nanodroplets, Nanoscale **12**, 20631 (2020).
[45] Y. Zhang, J. E. Sprittles, and D. A. Lockerby, Molecular simulation of thin liquid films: Thermal fluctuations and instability, Phys. Rev. E **100**, 023108 (2019).
[46] Y. Zhang, J. E. Sprittles, and D. A. Lockerby, Nanoscale thin-film flows with thermal fluctuations and slip, Phys. Rev. E **102**, 053105 (2020).
[47] X.-H. Li, X.-X. Zhang, and M. Chen, Estimation of viscous dissipation in nanodroplet impact and spreading, Phys. Fluids **27**, 052007 (2015).

[48] B.-X. Li, X.-H. Li, and M. Chen, Spreading and breakup of nanodroplet impinging on surface, Phys. Fluids **29**, 012003 (2017).
[49] Y.-F. Wang, Y.-B. Wang, F.-F. Xie, J.-Y. Liu, S.-L. Wang, Y.-R. Yang, S.-R. Gao, and X.-D. Wang, Spreading and retraction kinetics for impact of nanodroplets on hydrophobic surfaces, Phys. Fluids **32**, 092005 (2020).
[50] Y.-B. Wang, X.-D. Wang, Y.-R. Yang, and M. Chen, The maximum spreading factor for polymer nanodroplets impacting a hydrophobic solid surface, J. Phys. Chem. C **123**, 12841 (2019).
[51] Y.-B. Wang, Y.-F. Wang, S.-R. Gao, Y.-R. Yang, X.-D. Wang, and M. Chen, Universal model for the maximum spreading factor of impacting nanodroplets: From hydrophilic to hydrophobic surfaces, Langmuir **36**, 9306 (2020).
[52] S. Gao, Q. Liao, W. Liu, and Z. Liu, Nanodroplets impact on rough surfaces: A simulation and theoretical study, Langmuir **34**, 5910 (2018).
[53] Y.-B. Wang, Y.-F. Wang, Y.-R. Yang, X.-D. Wang, and M. Chen, Spreading time of impacting nanodroplets, J. Phys. Chem. C **125**, 5630 (2021).
[54] H. Li and K. Zhang, Dynamic behavior of water droplets impacting on the superhydrophobic surface: Both experimental study and molecular dynamics simulation study, Appl. Surf. Sci. **498**, 143793 (2019).
[55] F.-F. Xie, S.-H. Lv, Y.-R. Yang, and X.-D. Wang, Contact time of a bouncing nanodroplet, J. Phys. Chem. Lett. **11**, 2818 (2020).
[56] B.-X. Zhang, S.-L. Wang, and X.-D. Wang, Wetting transition from the Cassie–Baxter state to the Wenzel state on regularly nanostructured surfaces induced by an electric field, Langmuir **35**, 662 (2019).
[57] A. Giacomello, S. Meloni, M. Chinappi, and C. M. Casciola, Cassie–Baxter and Wenzel states on a nanostructured surface: Phase diagram, metastabilities, and transition mechanism by atomistic free energy calculations, Langmuir **28**, 10764 (2012).
[58] G. Pashos, G. Kokkoris, and A. G. Boudouvis, Minimum energy paths of wetting transitions on grooved surfaces, Langmuir **31**, 3059 (2015).
[59] X. He, B.-X. Zhang, S.-L. Wang, Y.-F. Wang, Y.-R. Yang, X.-D. Wang, and D.-J. Lee, Electrowetting-based control of wetting transition of a nanodroplet on pillar-arrayed surfaces, J. Mol. Liq. **345**, 117049 (2021).
[60] V. Molinero and E. B. Moore, Water modeled as an intermediate element between carbon and silicon, J. Phys. Chem. B **113**, 4008 (2009).
[61] See Supplemental Material at http://link.aps.org/supplemental/10.1103/PhysRevFluids.7.034203 for the validation of MD code.
[62] See Supplemental Material at http://link.aps.org/supplemental/10.1103/PhysRevFluids.7.034203 for the density distribution of an equilibrated nanodroplet.
[63] See Supplemental Material at http://link.aps.org/supplemental/10.1103/PhysRevFluids.7.034203 for the boundary points and fitting circles for the nanodroplets.
[64] M. A. Quetzeri-Santiago, A. A. Castrejón-Pita, and J. R. Castrejón-Pita, The effect of surface roughness on the contact line and splashing dynamics of impacting droplets, Sci. Rep. **9**, 15030 (2019).
[65] Y.-B. Wang, Y.-F. Wang, X. Wang, B.-X. Zhang, Y.-R. Yang, D.-J. Lee, X.-D. Wang, and M. Chen, Splash of impacting nanodroplets on solid surfaces, Phys. Rev. Fluids **6**, 094201 (2021).
[66] M. V. Chubynsky, K. I. Belousov, D. A. Lockerby, and J. E. Sprittles, Bouncing off the Walls: The Influence of Gas-Kinetic and van der Waals Effects in Drop Impact, Phys. Rev. Lett. **124**, 084501 (2020).
[67] M. A. Quetzeri-Santiago, J. R. Castrejón-Pita, and A. A. Castrejón-Pita, Controlling droplet splashing and bouncing by dielectrowetting, Sci. Rep. **11**, 21410 (2021).
[68] Y. Li, D. Quéré, C. Lv, and Q. Zheng, Monostable superrepellent materials, Proc. Natl. Acad. Sci. USA **114**, 3387 (2017).
[69] S. Chen, J. Wang, and D. Chen, States of a water droplet on nanostructured surfaces, J. Phys. Chem. C **118**, 18529 (2014).
[70] See Supplemental Material at http://link.aps.org/supplemental/10.1103/PhysRevFluids.7.034203 for the equilibrium wetting states of a nanodroplet on nanopillared surfaces with various intrinsic contact angles.
[71] See Supplemental Material at http://link.aps.org/supplemental/10.1103/PhysRevFluids.7.034203 for the impact regimes of nanodroplets onto nanopillared surfaces with various intrinsic contact angles.

[72] Y. D. Shikhmurzaev and J. E. Sprittles, Wetting front dynamics in an isotropic porous medium, J. Fluid Mech. **694**, 399 (2012).

[73] K. Kobayashi, K. Konno, H. Yaguchi, H. Fujii, T. Sanada, and M. Watanabe, Early stage of nanodroplet impact on solid wall, Phys. Fluids **28**, 032002 (2016).

[74] G. Zhang, M. A. Quetzeri-Santiago, C. A. Stone, L. Botto, and J. R. Castrejón-Pita, Droplet impact dynamics on textiles, Soft Matter **14**, 8182 (2018).